American Journal of Energy Research, 2024, Vol. 12, No. 3, 63-69
Available online at http://pubs.sciepub.com/ajer/12/3/3
Published by Science and Education Publishing
DOI:10.12691/ajer-12-3-3

CFD Investigation of the Effect of Multiple Phase Shift Angles on the Performance of a Two-Stage Savonius Wind Turbine

Susan Kariuki[1,*], Churchill Saoke[1], Joseph Kamau[2], Patrick Muiruri[3]

[1]Physics Department, Jomo Kenyatta University of Agriculture and Technology, Nairobi, Kenya
[2]Institute of Energy and Environmental Technology (IEET), Jomo Kenyatta University of Agriculture and Technology, Nairobi, Kenya
[3]Mechanical Engineering Department, Jomo Kenyatta University of Agriculture and Technology, Nairobi, Kenya
*Corresponding author: susannjoki164@gmail.com

Received October 10, 2024; Revised November 12, 2024; Accepted November 19, 2024

Abstract Wind is an alternative source of renewable energy following the current surge in energy demand globally. This is attributed to the worldwide call for the alleviation of the use of fossil fuel sources due to climate change. However, the larger part of the global coverage experiences low wind speed, inhibiting the application of medium and large wind turbines in harvesting wind energy with a return on investment. This leads to an increase in the application of small wind turbines. This study focused on studying the Savonius wind turbine, which is one of the potential candidates for harnessing wind energy efficiently in low wind speed areas. The study aimed to analyze the aerodynamic performance of a two-stage Savonius wind turbine using the Computational Fluid Dynamic (CFD) method by varying the phase shift angles (PSA) and tip speed ratio (TSR). The lower and upper rotors were designed such that the phase shift angles varied were 45^0, 60^0, 75^0 and 90^0. A Shear Stress Transport turbulence model SST k-omega with a steady-state method was used to analyze the influence of PSA and TSR on the performance of a two-stage Savonius wind turbine. The findings of this study indicated that the Savonius wind turbine with a PSA of 45^0 had the highest torque coefficient of 0.3654 at a TSR of 0.8 and a wind speed of 4m/s. Hence, phase shift angles significantly influence the performance of a two-stage Savonius wind turbine in low wind speed applications.

Keywords: *Phase shift angles, torque coefficient, tip speed ratio, computational fluid dynamics*

Cite This Article: Susan Kariuki, Churchill Saoke, Joseph Kamau, and Patrick Muiruri, "CFD Investigation of the Effect of Multiple Phase Shift Angles on the Performance of a Two-Stage Savonius Wind Turbine." *American Journal of Energy Research*, vol. 12, no. 3 (2024): 63-69. doi: 10.12691/ajer-12-3-3.

1. Introduction

Recently, the human population has exponentially grown, leading to a high demand for domestic and industrial energy consumption. A large amount of energy is currently generated from fossil sources, which negatively impact climate change, such as global warming, rise in temperature, and unpredictable rainfall patterns. Some authors [1] suggest that this is caused by the emission of greenhouse gases. In the long run, this advocates for the use of alternative energy sources, mainly renewable energy, such as hydro, tide, solar, biomass, geothermal, and wind. These sources have drawn a lot of attention from governments, private industries, and the research sector.

Wind energy is abundantly available and considered the least costly renewable energy source [2]. In relation to this, the popularity of wind energy has immensely grown in the last two decades, with countries such as China, the US, and Germany taking the lead in harvest of wind energy [3]. Wind turbine blades and wind vanes are known devices that convert kinetic energy in moving air to useful mechanical energy before changing it to electric power or other forms of consumable energy. The wind turbines are grouped based on the orientation of the rotational axis with reference to the ground surface. The two types of wind turbines are vertical axis wind turbines (VAWTs) and horizontal axis wind turbines (HAWTs). The HAWTs turbines' rotational axis is horizontal to the ground, while the VAWTs turbines' rotational axis is perpendicular to the ground.

Savonius wind turbines are VAWTs mainly used in electricity production and water pumping. One of the benefits brought in by the Savonius wind turbine is that it can operate under low wind speed, and this is attributed to its popularity in application to areas with low wind [4]. The turbine works best at low tip speed ratios (TSR) of between 0.6 and 0.8 [5,6], which contributes to their noiselessness, making them more acceptable in residential, urban, and rural areas. Additionally, these turbines have a high self-starting capability and can operate in turbulent wind conditions, which are mainly experienced in urban areas [7]. However, the fundamental flaw in these turbines' performance is their low efficiency and low power

generation compared to other turbines [4]. Additionally, the turbine produces negative torque within the ranges of 135^0 and 165^0 as well as between 315^0 and 345^0 [8].

These flaws have been the epitome of research, with various studies focusing on specific parameters that affect the turbine's performance, including the aspect ratio, overlapping ratio, end plate, number of blades, number of stages, blade material, and other augmentation geometric properties such as the use of smart blades, guide plates, and blade shape. Multi-stage turbines are viable in reducing negative torque, as evidenced by [9,10].

A comparison between a conventional and a two-stage turbine indicated that the latter performed better [11]. The conventional turbine, in this case, is referred to as a single-stage Savonius wind turbine, which is illustrated in Figure 1. In addition, a comparison between single-stage and two-stage Savonius wind turbines from various research conducted in helical turbines, hydrokinetic and elliptic turbines identified that the latter performs better [8,12,13].

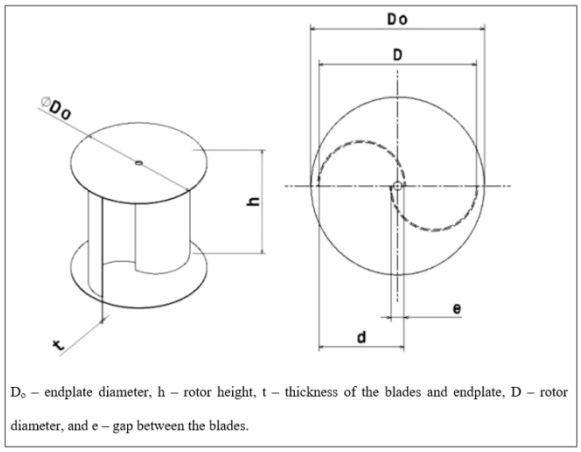

D_o – endplate diameter, h – rotor height, t – thickness of the blades and endplate, D – rotor diameter, and e – gap between the blades.

Figure 1. Conventional Savonius wind turbine [13]

A study by [14] revealed that a two-stage turbine with two blades performs better in terms of torque and power efficiency at a TSR of 0.6 than a two-stage turbine with either three or four blades. Investigation done numerically showed that the torque decreases with an increase in TSR [14]. Additionally, for all the turbines tested, the power output and power coefficient initially increased with an increase in TSR up to a peak of between 0.6 and 0.8 and later decreased with an increase in TSR [14]. An experimental and numerical study by [15] on a two-stage Savonius wind turbine, with the turbine being tilted at different angle positions. Their findings indicated that the torque coefficient (C_T) decreased with an increase in tip speed ratio (TSR).

Further, [16] investigated the aerodynamic performance of a two-stage Savonius wind turbine with twisted blades, and they concluded that the modifications of geometric parameters improved the overall performance of the turbine. However, these changes are lineated with complexing the structure of a Savonius turbine, and making it costly to maintain compared to the conventional two-stage Savonius wind turbine.

Various studies on multi-stage Savonius wind turbines have been numerically done using computational fluid dynamics (CFD). Numerical studies are used to verify and validate proposed wind turbine design concepts before building physical prototypes [18,19]. This allows innovative blade features and configurations to be evaluated efficiently through computational analysis. From the relevant literature reviewed, most studies focused on the comparison between single-stage and two-stage Savonius turbines. It revealed that the performance of the Savonius wind turbine depends on geometric parameters, positioning, and orientation of the blades. In conclusion, the reviewed literature calls for the design of an innovative turbine that can guarantee maximum power generation. This study, therefore, seeks to analyze how phase shift angles ranging between 45^0 and 90^0 affect the performance of a two-stage wind turbine.

2. Methodology

2.1. Working Station

All simulations were carried out using ANSYS version 2022 installed on a system having parallel processing with 8 core Intel ® i7-4510 u with 16 GB RAM.

2.2. Description of the Physical Model

The Savonius wind turbine under this study has two rotors, one on the lower stage and the other one on the upper stage, such that the two are superimposed on each other, which is then referred to as a two-stage Savonius wind turbine as shown in Figure 2. Both rotors have similar shapes, and all geometrical dimensions are the same for both lower and upper rotors. They are also aligned with the same orientation. The geometric dimensions of this wind turbine are tabulated in Table 1. This two-stage Savonius wind turbine is taken as the original wind turbine, and it is used to benchmark the findings obtained from this study.

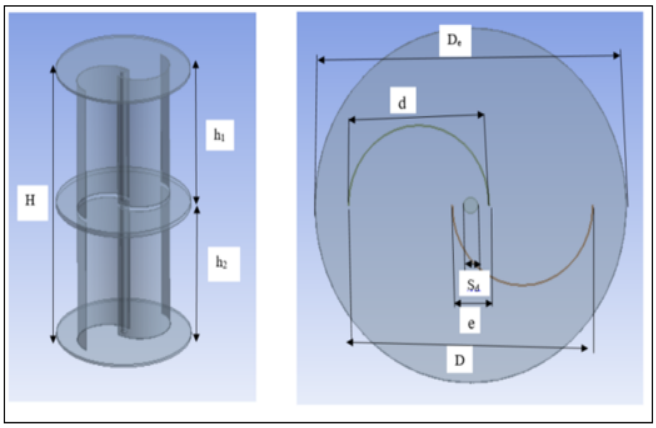

Figure 2. A two-stage Savonius wind turbine

Table 1. Showing dimensions of the geometries of the turbine

Dimensional Characteristics	Dimensions [mm]
Blade diameter (d)	170
Rotor diameter (D)	300
Rotor height (H)	600
Height of the upper rotor (h1)	300
Height of the lower rotor (h2)	300
Bucket gap width (s)	40
Radius of the blade (r)	85
The endplate diameter (D_e)	330

The orientation of the upper rotor was laterally rotated within angular angles ranging between 45^0 and 90^0. The shifting angular angle interval was kept at 15^o, and it is referred to as the phase shift angle (PSA) in this study. The various rotors are shown in Figures 3 and 4 below, both in 2D and 3D.

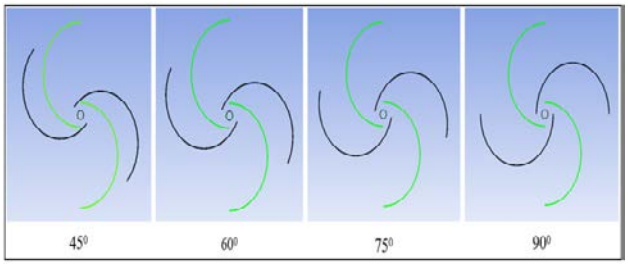

Figure 3. A 2-D view of the four turbines having varying phase shift angles, where the green blades are for the lower rotor while the black blades are for the upper rotor.

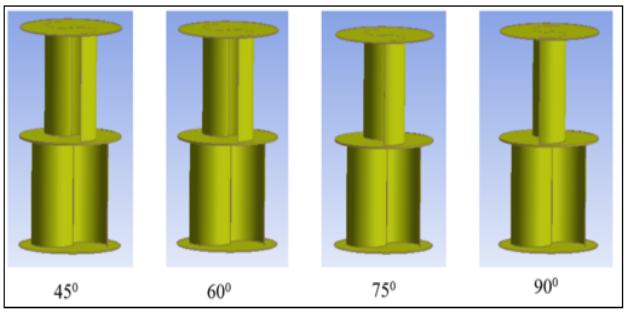

Figure 4. Two-stage Savonius wind turbines having varying phase shift angles.

The endplates (D_e) used have a circular profile where their diameters are kept constant and 1.1 of the rotor diameter (D). Each stage rotor created had its own endplates before being superimposed to form a two-stage turbine. The aspect ratio for each stage is 1, and the whole turbine is 2, as recommended by [16]. The overlapping ratio (s/d) for all the tested rotors is set at 0.16. All the rotors have a constant sweep area (A), where A = DH.

2.3. Computational Domain

The domain consists of stator domain and rotating domain as shown in Figure 5. The domains are separated using a sliding interface, ensuring the flow field continuity around the rotor. The measurements of domains are taken in multiples of the rotor diameter (D), where the measurements of the stator domain are 60D X 40D X 20D. The distance of the turbine center (0, 0, 0) to the inlet is 15D following recommendations by [19], which is in the brackets of a safe minimum distance to the inlet and avoids overestimation of the results. The distance to the outlet was set at 45D, which leads to a uniform outlet pressure coefficient. The diameter of the rotating domain was set at 1.5D. Overall, the size of the computational domain is maintained large enough to eliminate the effect of its boundaries on the performance of the rotor.

2.4. Meshing of Fluid Domain

In the present study, the fluid domain was discretized into small computational cells comprising unstructured tetrahedron elements. The stationary zone was meshed using the coarse elements, while the rotating domain and the turbine took up the finer mesh elements. The mesh generation process started with the edges, followed by faces and later body sizing to emulate the bottom-to-top strategy, and Figures 6 and 7 below show the mesh resolution. The quality of the elements was evaluated in terms of orthogonality quality and skewness. The quality of these elements was found to be in the range of 0 – 0.38 and 0.63 – 1.0 in terms of skewness and orthogonal quality, respectively. The mesh sizes were deemed of satisfactory quality with guaranteed reasonable accuracy, according to [20]. A mesh sensitivity test was conducted by considering six different mesh sizes on the stator domain, rotating domain, and blade surface. Refinement of the mesh was emphasized around the rotating domain and the blade surfaces.

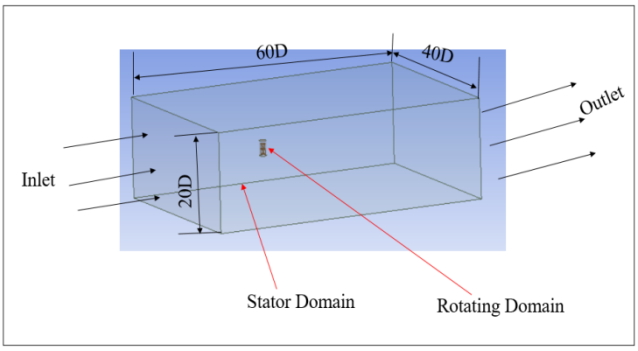

Figure 5. Computational domain

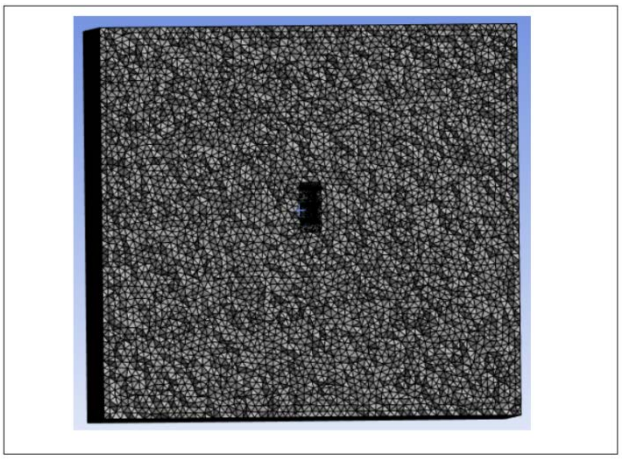

Figure 6. A cross-section of the computational domain (Stator and rotatory domain)

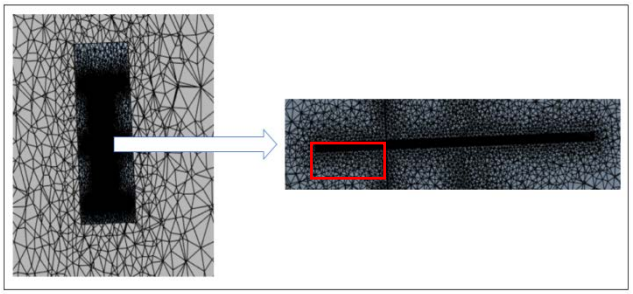

Figure 7. Cross-section of the rotatory domain showing parts of the turbine

2.5. Boundary Conditions

This study considered appropriate boundary conditions as they are necessary to obtain comprehensive results. In relation to this, the left and right boundary were assigned as inlet and outlet, where the inlet velocity was maintained at 4 m/s with a turbulent viscosity ratio and intensity of 10% and 5%, respectively. The inlet boundary was placed upstream of the rotor such that there was negligible effect on the inlet velocity profile. The outlet was assigned a pressure-based boundary condition, the gauge pressure was assigned zero, and a turbulence intensity of 1%. The surface of the blades is considered a rotatory wall and is assigned a no-slip boundary condition. The upper, lower, and lateral sides were assigned symmetry boundary conditions, such that the velocity normal to these sides was zero. The blades rotated at speeds corresponding to TSR values. As the wind turbine operated in an open atmosphere, the working fluid of the rotors under consideration was taken as air with a density of 1.225 kg/m^3 and a dynamic viscosity of 1.7894×10^{-5} Ns/m^2.

2.6. CFD Simulation

Computational Fluid Dynamics (CFD) method was used to perform all the simulations involved in this study. The methodology approach was borrowed from [21]. All the geometries and computational domains were developed using ANSYS Design Modeler, then they were subdivided into small finite volumes using ANSYS Mechanical mesh program. The computations were carried out using ANSYS Fluent. The finite volume method (FVM) was used in conjunction with the Reynolds Average Navier-Stoke (RANS) method, which was applied to solve and compute all the governing equations.

From Literature [16,22,23] SST $\kappa-\omega$ model, which combines the superior elements of $\kappa-\omega$ and $\kappa-\varepsilon$ turbulence models was selected as a closure to the governing equations. The first model is utilized in the inner part of the boundary layer. The $\kappa-\omega$ SST then switches to the standard $\kappa-\varepsilon$ in the core region of the flow, which is the wake region of the boundary layer and free shear layers. Another advantage that sets the $\kappa-\omega$ SST model apart is the eddy viscosity formulation, which is modified to take into account the effect of turbulent shear stress transportation, which is fundamental in predicting severe adverse pressure gradient flows.

The governing equations of the model are expressed as follows;

$$\frac{\partial \overline{u_i}}{\partial x_i} = 0 \tag{1}$$

$$\rho \frac{\partial \overline{u_i}}{\partial t} + \rho \frac{\partial}{\partial x_j}\left(\overline{u_i u_j} + \overline{u_i' u_j'}\right) = \frac{\partial P}{\partial x_i} + \frac{\partial \overline{\tau}_{ij}}{\partial x_j} + \rho f_i \tag{2}$$

where $\overline{u_i}$, ρ and P are the mean flow velocity components, density and pressure, respectively, x_i is the Cartesian coordinate and t is time. For the case of rotating reference the centrifugal and Coriolis are incorporated in the specific body force f_i and $\overline{\tau}_{ij}$ is the time-averaged viscous stress tensor components.

The closure SST $\kappa-\omega$ is expressed as shown in Eq. 3 and 4 below,

$$\frac{\partial}{\partial t}(\rho k) + \frac{\partial}{\partial x_i}(U_i \rho k) = \frac{\partial}{\partial x_j}\left((\mu + \sigma_k \mu_t)\frac{\partial}{\partial x_j} k\right) + \tilde{P}_k - \beta^* \rho \omega k. \tag{3}$$

$$\frac{\partial}{\partial t}(\rho\omega) + \frac{\partial}{\partial x_i}(U_i \rho \omega) = \frac{\partial}{\partial x_j}\left((\mu + \sigma_\omega \mu_t)\frac{\partial}{\partial x_j}\omega\right) + \frac{\rho\gamma}{\mu_t} S^2 - \beta\rho\omega^2 + 2\rho(1-F_1)\frac{1}{\omega}\frac{1}{\sigma_{\omega 2}}\frac{\partial}{\partial x_j}\omega. \tag{4}$$

where k is turbulent kinetic energy, S is the invariant measure of the strain rate, $\sigma_{\omega 2}$ is 0.856,

A Semi-Implicit Method for Pressure-Linked Equations (SIMPLE) algorithm was used to decouple velocity and pressure in a segregated manner. The convergence criterion of the x, y, and z velocities, k, and omega residuals was set at 10^{-5} apart from the residual for the continuity equation, which was set at 10^{-4}.

3. Results and Discussion

3.1. Performance Parameters

The primary parameters in this study are power coefficient, TSR and torque coefficient calculated using Eq. 5, 6 and 7.

$$C_P = \frac{P_{turbine}}{P_{available}} = \frac{T_{turbine} \times \omega_s}{\frac{1}{2}\rho A V^3} = C_T \times TSR \tag{5}$$

$$TSR(\lambda) = \frac{\omega d}{u} \tag{6}$$

$$C_T = \frac{T_{turbine}}{T_{available}} = \frac{T_{turbine}}{\frac{1}{2}\rho A V^3 R} \tag{7}$$

Where, $P_{available}$, $P_{turbine}$, $T_{turbine}$, $T_{available}$, A, R, V, u are power available, power generated at the rotor, torque generated by the rotor, torque available, area swept by rotor, radius of the rotor and free stream velocity and tip speed of the rotor, respectively.

3.2. Mesh Independence Study

Table 2 shows the amount of torque obtained for the six sets of mesh generated to determine the mesh size that strikes the balance between accuracy and computational rate. Figure 8 illustrates the performance of meshes with varying element sizes.

The results show that coarse elements resulted in poor performance compared to fine meshes. There was minimal torque difference for the mesh in case serial No. 4 as compared to obtained torque in mesh serial No. 5. In terms of mesh convergence, stability and computational rate, the mesh at serial No 4. was deemed satisfactory and it was

selected for this study.

Table 2. Torque generated versus element size

S/No	No. of Elements	No. of Nodes	Torque [N]
1	302792	56337	0.0421095
2	1706345	322979	0.0724265
3	1917723	359295	0.0725012
4	2479796	455810	0.0747887
5	2761834	501131	0.0749341
6	3016871	567428	0.0713724

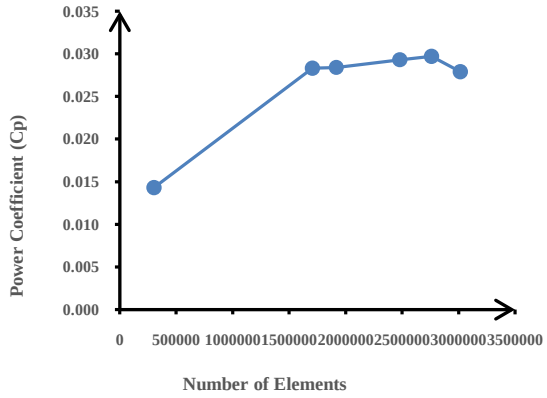

Figure 8. Trend of mesh sensitivity convergence in terms of the power coefficient

3.3. Validation of the Model

To validate the methodology adopted for simulation in this study, the first step was to attempt to replicate experimental data borrowed from [24], who used a conventional Savonius wind turbine having a gap width ratio of 0, aspect ratio of 1, and operating at Reynolds number 4.32 x 10^5. The results obtained from the CFD simulation were compared with the experimental data since the developed model emulates the same geometric designs as the experiment. The comparison of the results is shown in Figure 9 below.

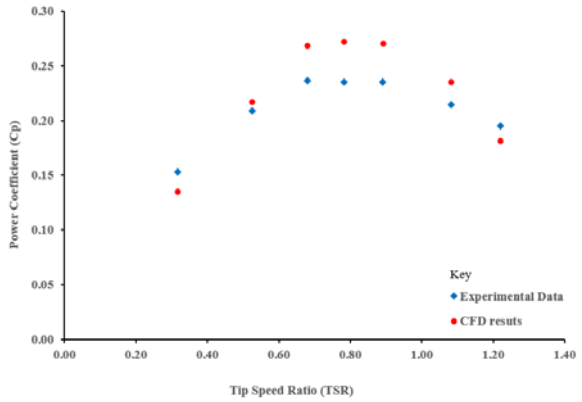

Figure 9. Validation results

From the results obtained and from Figure 9 above, the CFD results are in good agreement with the experimental data, where the mean absolute error is 6.974%, which was acceptable. These results also validated using the SST $\kappa-\omega$ turbulence model for the rest of the simulation. The deviation between experimental and CFD results could be due to inaccurate precision of the model geometry, material properties, and difficulty in quantifying and propagating uncertainties [25].

3.4. Torque Characteristics

The torque coefficient of all turbines with varying phase-shift angles was compared, and the results are shown in Figure 10 below.

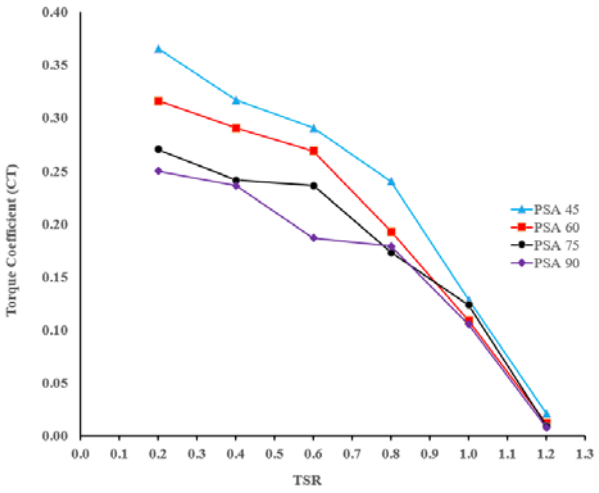

Figure 10. Torque coefficient against TSR

The turbine with a phase shift of 45^0 has the highest torque coefficient of 0.3654, while the turbine with a PSA of 90^0 has the lowest C_T of 0.2499. All the turbines had the highest C_T at a TSR of 0.2 where the C_T was 0.3654, 0.3164, 0.2706 and 0.2499 for turbines with PSAs of 45^0, 60^0, 75^0, and 90^0, respectively. The torque coefficient for all the turbines decreased with increasing TSR, such that the least C_T occurred at a TSR of 1.2, with the lowest Cm being 0.0081 for a turbine with a PSA of 90^0. This observation of a decreasing C_T with an increasing TSR on Savonius turbines was also noted by various researchers, including [14, 15]. The lowest C_T for other turbines were 0.0215, 0.0122 and 0.0098 for turbines with PSAs 45^0, 60^0 and 75^0, respectively.

At low TSR, the wind speed is much higher relative to the speed of the rotating blades. This creates a higher drag force on the concave side of the Savonius rotor blades as they push against the wind. This drag force is what creates the torque on the shaft. As TSR increases, the relative velocity between the wind and the blades decreases, reducing the torque, in turn reducing the torque coefficient. Compared to the rest of the turbines, for the PSA-45^0 turbines, the blades are positioned such that the advancing blade begins to capture the wind energy more effectively right after the previous blade has passed its peak torque position. This synchronization ensures a more continuous and smoother torque generation, minimizing the torque dips that can occur between blade transitions.

3.5. Power Characteristics

The power coefficients for all the turbines are graphically represented in Figure 11 below. The turbine with PSA 45^0 performed the best, with a power coefficient of 0.1923 at a TSR of 0.8. Two of the turbines with PSAs

45^0 and 90^0, had their best performance at a TSR of 0.8, with the highest Cp of the latter being 0.1434. For the turbine with a PSA of 45^0 there is a minimal angular displacement or phase shift between the lower and upper stage compared to other turbines tested. This allows for a more continuous and smooth interaction with the wind, reducing the amount of turbulent flow and leading to more consistent aerodynamic forces on the blades.

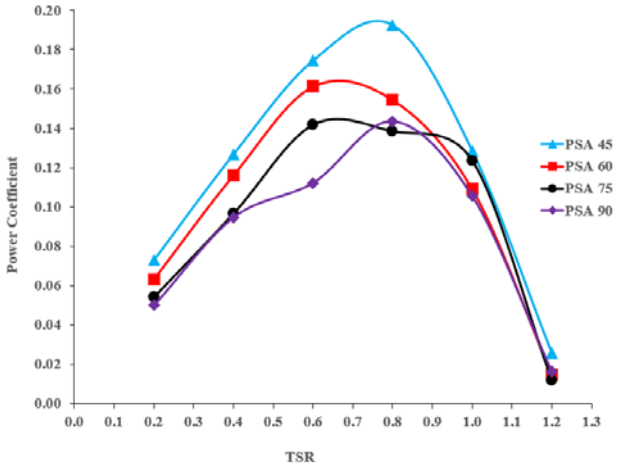

Figure 11. Power coefficient against tip speed ratio

The rest of the turbines with PSAs 60^0 and 75^0 had their best performance at TSR 0.6, where the Cps were 0.1613 and 0.1419, respectively. The turbine with PSA 75^0 had the lowest performance compared to other turbines, with a discrepancy of 15.08% from the highest Cp recorded. The Cps for all the turbines increased with an increasing TSR until at certain points, 0.6 and 0.8, before decreasing with increasing TSR, a case also observed by [5,26].

The power coefficient of a wind turbine increases with increasing tip speed ratio up to an optimal point in this study, 0.6 and 0.8, due to improved aerodynamic efficiency and reduced flow separation. Beyond this optimal TSR, the power coefficient starts to decrease because of increased drag forces, unfavorable angle of attack, and mechanical limitations.

3.6. Velocity and Pressure Contours

Figure 12 and Figure 13 show the contours for all turbines for the upper and lower rotor.

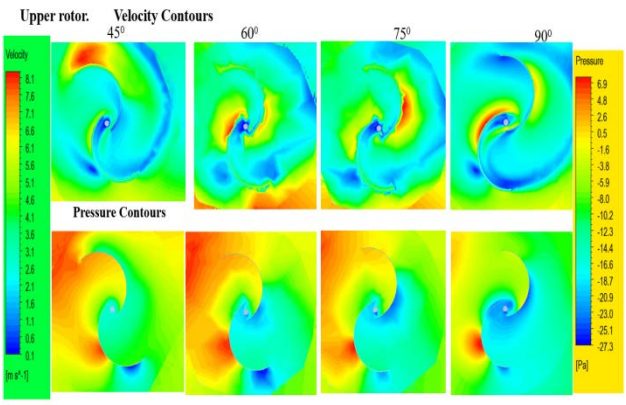

Figure 12. Velocity and pressure contours for the upper rotors of all the turbines

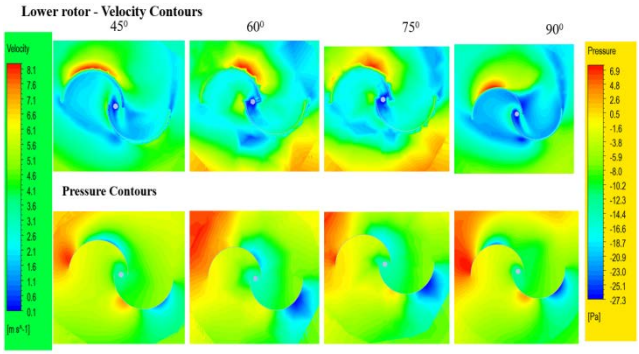

Figure 13. Velocity and pressure contours for the upper rotors of all the turbines

From Bernoulli's principle, velocity and pressure are inversely proportional, and this is evident from velocity and pressure contours shown in Figure 12 and Figure 13 for both the lower and upper stage rotors. Significant changes in velocity and pressure contours on the upper-stage rotors were caused by changes in phase shift angles. The turbine with PSA 45^0 had a higher pressure gradient when compared to all the turbines studied, hence, its high performance.

4. Conclusion

A series of numerical simulations were conducted to investigate the impact of phase shift angles (45^0, 60^0, 75^0, and 90^0) on the performance of a two-stage Savonius wind turbine using (CFD). The analysis employed ANSYS software and the SST k-ω turbulence model. The results revealed a significant influence of phase shift angle on the turbine's power and torque coefficients, which are key metrics for wind energy conversion efficiency. The configuration with a phase shift angle of 45° achieved the highest Cp and C_T values of 0.19 and 0.3654. The turbine with a phase shift angle of 75° resulted in the lowest Cp of 0.1419 at its peak TSR of 0.6. The observed trends can be attributed to the interaction between the blade profiles of the two stages at different phase shifts. These findings highlight the importance of optimizing phase shift angle for maximizing the power output of two-stage Savonius wind turbines.

References

[1] M. Kabir *et al.*, "Climate change due to increasing concentration of carbon dioxide and its impacts on environment in 21st century; a mini review," *J. King Saud Univ.-Sci.*, vol. 35, no. 5, p. 102693, 2023.

[2] T. R. Ayodele and A. S. O. Ogunjuyigbe, "Wind energy resource, wind energy conversion system modelling and integration: a survey," *Int. J. Sustain. Energy*, vol. 34, no. 10, pp. 657–671, Nov. 2015.

[3] M. Ebrahimpour, R. Shafaghat, R. Alamian, and M. Safdari Shadloo, "Numerical investigation of the Savonius vertical axis wind turbine and evaluation of the effect of the overlap parameter in both horizontal and vertical directions on its performance," *Symmetry*, vol. 11, no. 6, p. 821, 2019.

[4] D. W. Wekesa, C. O. Saoke, and J. N. Kamau, "An experimental investigation into performance characteristics of H-shaped and Savonius-type VAWT rotors," *Sci. Afr.*, vol. 10, p. e00603, 2020.

[5] K. K. Sharma, R. Gupta, and A. Biswas, "Performance measurement of a two-stage two-bladed Savonius rotor," *Int. J. Renew. Energy Res.*, vol. 4, no. 1, pp. 115–121, 2014.

[6] J. Yao, F. Li, J. Chen, Z. Yuan, and W. Mai, "Parameter analysis of Savonius hydraulic turbine considering the effect of reducing flow velocity," *Energies*, vol. 13, no. 1, p. 24, 2019.

[7] C. B. K. Sampurno, D. D. P. Tjahjana, and S. Hadi, "The use of phase shift angle (PSA) on double stage savonius wind rotor with three points configuration semi-elliptical blade shape," in *IOP Conference Series: Earth and Environmental Science*, IOP Publishing, 2019, p. 012004. Accessed: Jul. 25, 2024. [Online]. Available: https:// iopscience.iop.org/ article/ 10.1088/ 1755-1315/345/1/012004/meta.

[8] S. Seralathan, P. S. Kumar, S. Singh, R. Raj, and S. Sathish, "Numerical analysis of the one-stage and two-stage helical Savonius vertical axis wind turbine," in *AIP Conference Proceedings*, AIP Publishing, 2022. Accessed: Jul. 25, 2024. [Online]. Available: https://pubs.aip.org/aip/acp/article-abstract/2385/1/120005/2820572.

[9] A. S. Saad, S. Ookawara, and M. Ahmed, "Influence of varying the stage aspect ratio on the performance of multi-stage Savonius wind rotors," *J. Energy Resour. Technol.*, vol. 144, no. 1, p. 011301, 2022.

[10] M. A. Kamoji, S. B. Kedare, and S. V. Prabhu, "Experimental Investigations on Two and Three Stage Modified Savonius Rotor," *Wind Eng.*, vol. 35, no. 4, pp. 483–509, Aug. 2011.

[11] D. E. Ohaji, M. Musa, M. Momoh, D. O. Akpootu, and G. Bello, "CONSTRUCTION AND PERFORMANCE EVALUATION OF TWO STAGED THREE BLADED SAVONIUS VERTICAL AXIS WIND ENERGY CONVERSION SYSTEM," *FUDMA J. Sci.*, vol. 6, no. 6, pp. 76–88, 2022.

[12] U. K. Patel, N. Alom, and U. K. Saha, "Aerodynamic analysis of a 2-stage elliptical-bladed Savonius wind rotor: Numerical simulation and experimental validation," *Int. J. Green Energy*, vol. 21, no. 1, pp. 102–115, Jan. 2024.

[13] F. Wenehenubun, A. Saputra, and H. Sutanto, "An experimental study on the performance of Savonius wind turbines related with the number of blades," *Energy Procedia*, vol. 68, pp. 297–304, 2015.

[14] M. S. M. Halmy, D. H. Didane, L. O. Afolabi, and S. Al-Alimi, "Computational fluid dynamics (cfd) study on the effect of the number of blades on the performance of double-stage savonius rotor," *Cfd Lett.*, vol. 13, no. 4, pp. 1–10, 2021.

[15] L. B. Kothe and A. P. Petry, "Numerical and Experimental Study of a Two-Stage Savonius Wind Turbine," *Rev. Eng. Térmica*, vol. 18, no. 2, pp. 52–61, 2019.

[16] A. S. Saad, A. Elwardany, I. I. El-Sharkawy, S. Ookawara, and M. Ahmed, "Performance evaluation of a novel vertical axis wind turbine using twisted blades in multi-stage Savonius rotors," *Energy Convers. Manag.*, vol. 235, p. 114013, 2021.

[17] X. Chen, Z. Qin, K. Yang, X. Zhao, and J. Xu, "Numerical analysis and experimental investigation of wind turbine blades with innovative features: Structural response and characteristics," *Sci. China Technol. Sci.*, vol. 58, no. 1, pp. 1–8, Jan. 2015.

[18] P. Veers *et al.*, "Grand challenges in the design, manufacture, and operation of future wind turbine systems," *Wind Energy Sci.*, vol. 8, no. 7, pp. 1071–1131, 2023.

[19] A. Rezaeiha, H. Montazeri, and B. Blocken, "Towards accurate CFD simulations of vertical axis wind turbines at different tip speed ratios and solidities: Guidelines for azimuthal increment, domain size and convergence," *Energy Convers. Manag.*, vol. 156, pp. 301–316, 2018.

[20] N. Fatchurrohman and S. T. Chia, "Performance of hybrid nano-micro reinforced mg metal matrix composites brake calliper: simulation approach," in *IOP conference series: materials science and engineering*, IOP Publishing, 2017, p. 012060. Accessed: Jul. 25, 2024. [Online]. Available: https:// iopscience.iop.org/ article/ 10.1088/1757-899X/257/1/012060/meta.

[21] P. I. Muiruri, O. S. Motsamai, and R. Ndeda, "A comparative study of RANS-based turbulence models for an upscale wind turbine blade," *SN Appl. Sci.*, vol. 1, no. 3, p. 237, Mar. 2019.

[22] F. Balduzzi, A. Bianchini, R. Maleci, G. Ferrara, and L. Ferrari, "Critical issues in the CFD simulation of Darrieus wind turbines," *Renew. Energy*, vol. 85, pp. 419–435, 2016.

[23] M. Oneissi, C. Habchi, S. Russeil, D. Bougeard, and T. Lemenand, "Novel design of delta winglet pair vortex generator for heat transfer enhancement," *Int. J. Therm. Sci.*, vol. 109, pp. 1–9, 2016.

[24] R. E. Sheldahl, B. F. Blackwell, and L. V. Feltz, "Wind tunnel performance data for two- and three-bucket Savonius rotors," *J. Energy*, vol. 2, no. 3, pp. 160–164, May 1978.

[25] Y. Tominaga, L. L. Wang, Z. J. Zhai, and T. Stathopoulos, "Accuracy of CFD simulations in urban aerodynamics and microclimate: Progress and challenges," *Build. Environ.*, p. 110723, 2023.

[26] N. M. Ali, A. A. Hassan, and S. Aljabair, "Effect of conventional multistage savonius wind turbines on the performance of the turbine at low wind velocity," *Jour Adv Res. Dyn. Control Syst.*, vol. 11, no. 11, 2019, Accessed: Jul. 24, 2024. [Online]. Available: https://www.academia.edu/download/85811391/JARDCS_vol_11_No._11_effect_of_conventional_Savonius.pdf.